

Positronium emission spectra from self-assembled metal-organic frameworks

P. Crivelli,^{1,*} D. Cooke,¹ B. Barbiellini,² B. L. Brown,³ J. I. Feldblyum,^{4,5} P. Guo,⁴ D. W. Gidley,⁶ L. Gerchow,¹ and A. J. Matzger⁴

¹*Institute for Particle Physics, ETH Zurich, Switzerland*

²*Department of Physics, Northeastern University, Boston, Massachusetts 02115, USA*

³*Department of Physics, Marquette University, Milwaukee, Wisconsin 53233, USA*

⁴*Department of Chemistry, University of Michigan, Ann Arbor, Michigan 48109, USA*

⁵*Macromolecular Science and Engineering, University of Michigan, Ann Arbor, Michigan 48109, USA*

⁶*Department of Physics, University of Michigan, Ann Arbor, Michigan 48109, USA*

(Received 4 October 2013; revised manuscript received 20 May 2014; published 18 June 2014)

Results of positronium (Ps) emission into vacuum from self-assembled metal-organic frameworks (MOFs) are presented and discussed in detail. Four different MOF crystals are considered, namely, MOF-5, IRMOF-8, $\text{ZnO}_4(\text{FMA})_3$, and IRMOF-20. The measurements reveal that a fraction of the Ps is emitted into vacuum with a distinctly smaller energy than what one would expect for Ps localized in the MOFs' cells. Only calculations considering the Ps delocalized in a Bloch state can reproduce the measured Ps emission energy providing a robust demonstration of wave function delocalization in quantum mechanics. We show how the Bloch state population can be controlled by tuning the initial positron beam energy. Therefore, Ps in MOFs can be used both to simulate the dynamics of delocalized excitations in materials and to probe the MOFs for their advanced characterization.

DOI: [10.1103/PhysRevB.89.241103](https://doi.org/10.1103/PhysRevB.89.241103)

PACS number(s): 36.10.Dr, 78.70.Bj, 81.05.Rm

Positronium (Ps), the bound state of the electron and its antiparticle (the positron), is the lightest atom in nature, which has inspired many fascinating studies [1–7] in fundamental and applied research. In particular, Ps delocalization in a Bloch state is a rare phenomenon that can only be observed in a few crystals such as quartz. Historically, Brandt *et al.* [8] discovered spectacular fine structure in the electron-positron momentum density of quartz, while Greenberger *et al.* [9] demonstrated that this feature is the manifestation of Ps formation in the form of a Bloch state. The same phenomena was also observed in alkali halides [8,10]. In both quartz and halides, the positron wave function strongly overlaps with electrons outside the Ps. Therefore, the annihilation with electrons having an antiparallel spin reduces the ortho/triplet Ps lifetime to only several hundred picoseconds [11]. To comprehensively study and use Ps Bloch waves it is highly desirable to expand this lifetime.

Evidence for Ps Bloch states living tens of nanosecond in self-assembled metal-organic frameworks (MOFs) has recently been reported [12]. MOFs are formed from the self-assembly of metal atoms or clusters linked by organic ligands (“linkers”) in highly regular structures with nanometer lattice size. The results are materials with extremely porous lattices and having surface areas up to and exceeding 7000 m²/g [13,14]. Development has been driven by interest in industrial application of such highly sorbent materials to catalysis and gas (particularly hydrogen) storage (e.g., [15]). By studying the emission probability of Ps escaping from large MOF grains Dutta *et al.* [12] deduced record-long Ps diffusion lengths that increased at lower temperatures, consistent with Ps existing primarily as a delocalized (Bloch) state in the lattice.

In this Rapid Communication we take advantage of a monoenergetic positron beam to control the depth of Ps formation below the MOF grain surface. This enables us to

definitively demonstrate the existence of a long-lived Ps Bloch wave in MOF by studying the depth-profiled energy spectrum of Ps emitted into vacuum from four MOFs with different lattice parameter: $\text{ZnO}_4(\text{FMA})_3$ (hereafter, FMA) [16], MOF-5 [17], IRMOF-8 [18], and IRMOF-20 [19]. As we will show, the emission spectrum provides a direct view of the state energies available to Ps in the lattice at the moment of its emission into vacuum. Most importantly, the Ps Bloch state has a distinguishably low energy that can be easily resolved from the energies of the Ps states that are confined in a given MOF cell.

All these MOFs are based on the ZnO_4 cluster, and thus form an *isoreticular* series (hence IRMOF) in which cell dimensions change according to the length of the chosen linker. The cluster-to-cluster distance (L) and the minimum side of the aperture (a), defined as the distance from the *closest* hydrogen atoms on opposite sides of the framework (Fig. 1) are reported in Table I.

For this study we used the ETHZ slow e^+ beam [20,21]. The slow positrons from the beam are accelerated to 1–20 keV towards the MOF target. After implantation, the e^+ can either form Ps (o-Ps or p-Ps), or annihilate into 2γ rays directly. Positron implantation is tagged by detection of secondary electrons (SE), generated when the e^+ hit the target, with a microchannel plate (MCP). This provides the start time (t_0) to build the time distributions used to measure the yield and energy of Ps emitted into vacuum and lifetime of Ps in the MOF frameworks. The stop is given by the annihilation photons detected with the detectors mounted around the target region [21,22].

The MOF crystals, synthesized at the University of Michigan, typically have grain sizes of 300 μm and cells of 1–1.5 nm (see Table I). The mean e^+ implantation depth, estimated using a Makhovian profile [23], is $\sim 0.5 \mu\text{m}$ for an e^+ implantation energy of 5 keV, rising to $\sim 3 \mu\text{m}$ for 15 keV. The positrons implanted in the MOF target rapidly thermalize through collisions with molecules of the MOF framework;

*crivelli@phys.ethz.ch

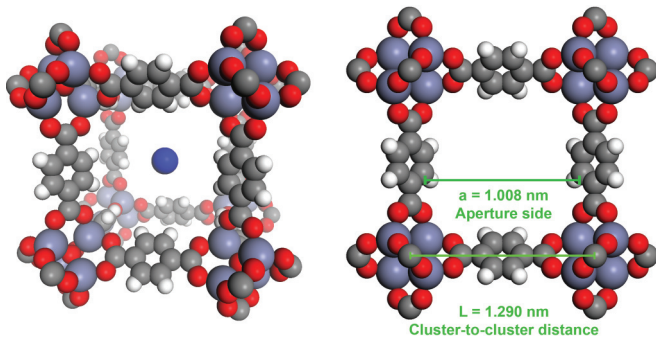


FIG. 1. (Color online) Schematic representation of Ps and cluster-to-cluster distance and aperture side in MOF-5.

a fraction of these form Ps. The large positron conversion efficiency suggests that the Ps forms directly by either Ore or spur processes in the MOF as it would in a molecular gas [24]. MOFs have framework sizes of the order of 1 nm, which is comparable with the Ps de Broglie wavelength for the energy range of interest. Therefore, Ps behavior in MOFs has to be treated quantum mechanically as in porous silica films with 3–4-nm pores [21,25] and its diffusion is expected to proceed via tunneling (as for muonium [26]).

The energy of the Ps emitted into vacuum will depend on the positron implantation energy since this determines the depth at which Ps formation occurs (see Fig. 2). Ps diffusing from greater depths has a higher probability of losing energy by phonon scattering and thus populates the lowest available energy states just prior to emission (see Fig. 3). At room temperature, after sufficient thermalization time only the ground state should be populated as in the case of silica [21,25], so for high e^+ implantation energy, one should expect to observe Ps with lowest energies in the range of 250–400 meV. To set this bound we use the cluster-to-cluster distance of the MOFs reported in Table I assuming Ps in an infinite well.

From the time distributions we determine the yield of Ps emitted into vacuum in the usual way, performing a fit of the long exponential corresponding to the Ps lifetime in vacuum [27]. We define the Ps vacuum yield as the probability of Ps emission into vacuum per implanted e^+ . For more than 5 kV, Ps is assumed to be thermalized thus the diffusion length is constant. By fitting the vacuum yield curves we can determine the diffusion lengths of Ps in the various MOFs [25]. These values are shown in Table I, and are in agreement with those extracted using a different experimental technique [12].

TABLE I. Density (ρ), cluster-to-cluster distance (L), aperture side (a), Ps diffusion length (l_{Ps}), and Ps lifetime (τ_{MOF}) of the MOF frameworks for the studied samples. The fact that the diffusion lengths are longer for the material with smaller holes can be understood because of the wavelike behavior of Ps in MOFs (see text for more details).

Sample	ρ (g/cm ³)	L (nm)	a (nm)	l_{Ps} (μ m)	τ_{MOF} (ns)
IRMOF-20	0.511	1.469	1.184	3.0 ± 0.2	20 ± 1
IRMOF-8	0.448	1.505	1.101	2.4 ± 0.2	18 ± 1
MOF-5	0.593	1.290	1.008	6.3 ± 0.4	13 ± 1
FMA	0.812	1.082	0.875	9.3 ± 5.5	10 ± 1

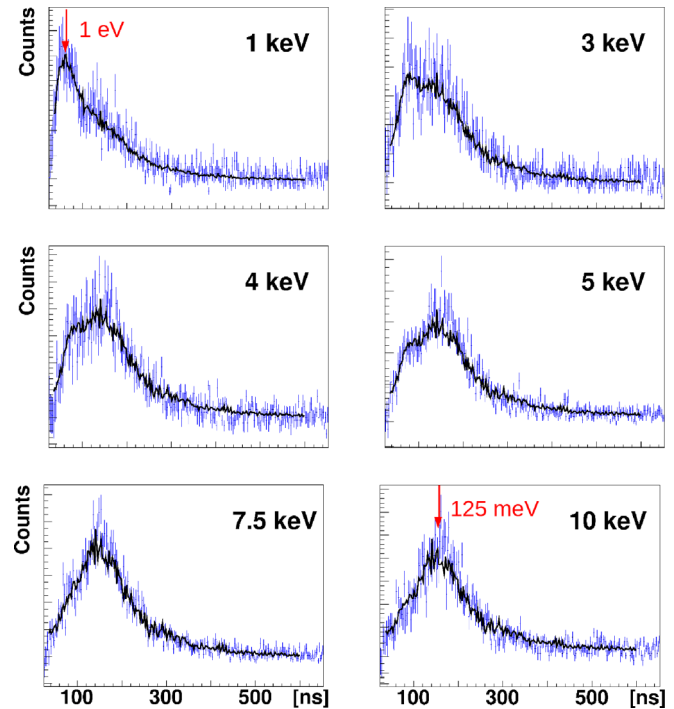


FIG. 2. (Color online) TOF spectra for MOF-5 fitted to the simulation as explained in the text. For comparison the time for a Ps emitted perpendicular to the surface with 125 meV to reach the center of the collimator slit (20 mm) is 150 ns.

To determine the emission energy of Ps into vacuum we fit the measured time-of-flight (TOF) distributions with a sum of spectra simulated with the GEANT4 code [21,28]. We use monoenergetic distributions emitted isotropically with their fractions as the free parameters. Our choice is justified by the fact that Ps in the MOF pores can only occupy discrete energy levels. Higher emission energies (corresponding to unbound Ps) are not well resolved by the TOF detector, and so may be

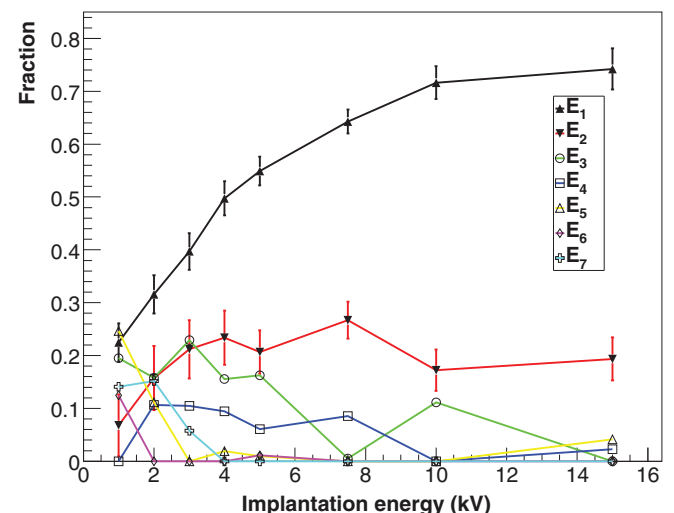


FIG. 3. (Color online) Evolution of the different energy components in MOF-5 (and typical of the other three MOF's [22]) as a function of the e^+ implantation energy. For readability only the error of the first two components is presented.

TABLE II. Observed energy components (in meV) for the different MOFs.

Sample	E_1	E_2	E_3	E_4	E_5	E_6	E_7
IRMOF-20	120 ± 10	250 ± 50	500 ± 50	700 ± 50	900 ± 50	1100 ± 50	1500 ± 100
IRMOF-8	138 ± 15	300 ± 50	600 ± 50	800 ± 50	1200 ± 50	1400 ± 50	1800 ± 100
MOF-5	125 ± 5	300 ± 50	600 ± 50	800 ± 50	1050 ± 50	1300 ± 50	1800 ± 100
FMA	162 ± 5	400 ± 50	800 ± 50	1200 ± 50	1500 ± 50	1800 ± 100	2400 ± 100

approximated by a sum of several monoenergetic distributions. The best fits at the lowest e^+ implantation energies are achieved with six or seven energy distributions (see Table II). At high energies e^+ (7.5–10 kV) only two or three of the lowest Ps energy components are found. The best fits give the same values within the quoted errors for all the different e^+ implantation energies we measured. Typical reduced χ^2 are of the order of 1–1.15 for 230 degrees of freedom depending on the e^+ implantation energy. As a cross-check we took data at different slit positions (10, 15, and 20 mm) achieving consistent results. From these measurements, one can also determine the delay time for Ps emission into vacuum due to the diffusion to the surface [29,30]. This can be estimated by extrapolation to a slit position of 0 mm. We obtain values in the range from a few nanoseconds up to 15 ns depending on the sample for implantation energies of 10 kV. We do not correct for this time (<10% of the TOF time) in the determination of the emission energy but this effect is included in the quoted error. Table II summarizes the observed energy components for the four MOFs. In Fig. 2 we show the TOF spectra of MOF-5 for different e^+ implantation energies. The fraction of Ps emitted with the lowest energy E_1 (shown in Fig. 3 for MOF-5) dominates as deeper positron implantation promotes Ps thermalization.

Strikingly, the lowest energy component E_1 given in Table II is about a factor of 2 smaller than the ≈ 300 meV ground-state energy expected for a Ps confined in the MOF cell. As we will show, this low value can be understood only if the Ps becomes a delocalized Bloch wave propagating in the periodic structure of the MOF.

A single cell of MOF (side L) is connected to neighboring cells via apertures of width a , where $a < L$. A Ps, because of its large zero point motion, occupies all the MOF cell homogeneously and its wave-function spillover in the “forbidden” channel aperture along the x direction is given by the semiclassical exponential decay [31] $\exp(-p_x x)$, where $p_x = \sqrt{2\pi}/a$ is the transverse confinement momentum for the square aperture of size a . Thus, the Ps spillover in the x direction is equivalent to a one-dimensional quantum-mechanical problem in an effective potential barrier with a potential height V_0 :

$$V_0 = \frac{\hbar^2 \pi^2}{ma^2}, \quad (1)$$

where m is the Ps mass and \hbar the reduced Planck constant. The same argument applies to the apertures along the y and z directions. Therefore, we can model the MOF’s porous lattice with empty cubes of side a separated by walls $b = L - a$ thick with confinement potential V_0 as shown in Fig. 4.

The actual MOF potential is clearly different. Nevertheless, this type of shape approximation is routinely used in band-structure calculations (see, e.g., [32]), and it still gives very

reliable results. The reason is because the exact shape of the potential in the interstitial region is not important given the long wavelengths of both the valence electrons and Ps. The *cubic muffin tin model* illustrated in Fig. 4 is exactly solvable since in each direction (x, y, z) it reduces to the well-known Kronig-Penney problem. We can thus calculate the expected emission energy of a Ps in a Bloch state with

$$\frac{\gamma^2 - \beta^2}{2\beta\gamma} \sinh(\gamma b) \sin(\beta a) + \cosh(\gamma b) \cos(\beta a) = \cos[k(a + b)], \quad (2)$$

where $\gamma = \kappa\sqrt{V_0 - E}$, $\beta = \kappa\sqrt{E}$, $\kappa = \sqrt{(2m)/\hbar^2}$, and the wave vector $k = 0$ [33].

The second column of Table III presents the values of the box size a required to reproduce the lowest experimental emission energy E_1 given in Table II. The fact that our deduced box sizes are consistent with Table I (i.e., these values are comparable or slightly larger than the minimum aperture side lengths for all four MOFs) confirms the reliability and robustness of the cubic muffin tin approximation. Higher lying Bloch states (i.e., excited bands) are too fragile to exist because of the decoherence by phonons: An intense level of scattering of an excited Ps with phonons would give the incoherent limit beyond which Bloch-wave propagation becomes inhibited.

As a result of its decoherence, the Ps becomes “nearsighted” and only sees a finite square well of width a and depth V_0 . The Ps bound states in the well can be calculated by solving a simple Schrödinger equation for each direction (x, y, z) giving the following conditions:

$$\sqrt{u_0^2 - v^2} = \begin{cases} v \tan v & \text{(symmetric case)} \\ -v \cot v & \text{(antisymmetric case)} \end{cases}, \quad (3)$$

where $v = ak/2$ and $u_0^2 = ma^2 V_0 / 2\hbar^2 = \pi^2/2$. In this case there are two solutions: $v_1 = 1.06$ and $v_2 = 2.01$. The energy levels of the four possible nondegenerate bound states in the

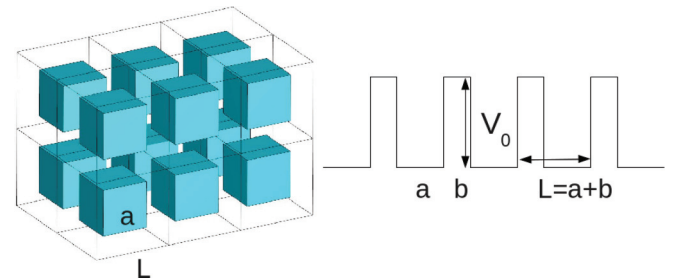


FIG. 4. (Color online) Cubic muffin tin geometry of the MOFs and Kronig-Penney potential.

TABLE III. Calculated energy levels (in meV) for the different MOF structures for a given side length a .

Sample	a (nm)	BS	E_{111}	E_{211}	E_{221}	E_{222}
IRMOF-20	1.17 ± 0.02	122 ± 10	188	350	512	675
IRMOF-8	1.15 ± 0.03	139 ± 15	194	362	530	699
MOF-5	1.08 ± 0.01	122 ± 5	220	411	603	794
FMA	0.91 ± 0.01	168 ± 5	311	580	849	1118

three-dimensional finite potential well are given by

$$E_{ijk} = \frac{2\hbar^2}{ma^2}(v_i^2 + v_j^2 + v_k^2) \quad \text{for } i, j, k \in \{1, 2\}. \quad (4)$$

The columns 4–7 of Table III are the Ps energies calculated using Eq. (4) for a potential well of side a given in column 2 and height V_0 . By comparing Tables II and III, it appears that our measurements cannot resolve well the E_{111} and the E_{211} levels, which are merged in the E_2 component. However, the E_{221} and the E_{222} energy levels are well reproduced by the E_3 and E_4 components for all the measured samples. Above E_4 no bound state can exist, therefore we identify the sum of the E_5 , E_6 , and E_7 components as an approximation of the continuum. Figure 3 can thus be viewed as the population evolution of the Ps quantum states in the lattice as it thermalizes: the Bloch states (E_1), the localized states (E_2 – E_4), and the continuum states ($-E_7$) (see also [22]).

It might be argued that E_1 is not a quantum state of Ps in the lattice but the result of some unknown inelastic process working on the higher energy states E_2 , E_3 , etc., that are the correct quantum states of Ps. The putative inelastic channel must have some branching ratio from E_2 or E_3 (the higher states are too low in population) such that the only way the intensity of E_1 can increase is if the population of these parent states increases as well. The populations of the E_2 and E_3 states do not parallel the increase in the E_1 component in Fig. 3 (the same is true for the other MOFs as shown in [22]). This inconsistency with inelastic scattering coupled with the large asymptotic rise in E_1 occupation for deeper Ps implantation definitively demonstrates that E_1 is the energy of the fundamental ground state of Ps in the MOF lattice.

The observed Ps localized states given by Eq. (4) can be understood in terms of the decoherence produced by the scattering with phonons. A simple explanation of the Ps localization mechanism can be formulated in terms of the Anderson condition [34] comparing the variations of the on-site energy δV with the Ps energy bandwidth (BW). A hot Ps interacting with the lattice can easily emit phonons producing variations of on-site energy δV associated with vibration of the box. If $\delta V/\text{BW} \gg 1$ the Ps localizes [35].

Only when Ps has dissipated all its energy to emit phonons such that $\delta V > \text{BW}$ can its migration be wavelike [36].

The *depth-profiled* Ps yield and emission energy measurements herein provide the requisite complementary evidence to [12] to definitively conclude that the Ps ground state in the IRMOF series is a Bloch state. To summarize, we independently confirm the unusually long diffusion lengths reported in [12]. Then we show that the lowest component of the Ps emission energy spectrum for all four MOFs is inconsistent with any inelastic scattering mechanism and is too low in energy to be due to Ps localized in the MOF cells. This low energy emission is clearly explained within a robust cubic muffin tin model for a Ps Bloch state in each different-sized MOF. By tuning the positron implantation energy, the evolution of the Ps occupation numbers in different states provides a control experiment wherein the lowest energy component disappears when the Bloch state occupation is likely to be disrupted. Hence, Ps atoms in MOFs can be used to understand the exciton migration in molecular crystals, which can be either wavelike (coherent) or diffusionlike (incoherent) [37,38]. In the case of the MOFs, the Ps lives much longer and diffuses over relatively large distances (10 μm) compared to alkali halides [39], therefore the migration study is considerably facilitated. Thus, such analogy between excitons and Ps could provide a complementary approach to cold atom simulators [40] to solve complicated condensed matter problems, e.g., the mechanism of photosynthetic light harvesting units [41]. Moreover, from a practical point of view, the relative populations of Bloch state and localized Ps might be used to ascertain the extent of interconnectivity in a porous framework. This may be especially useful to quantify trapped atoms or molecules in the cells or local pore collapse, inhomogeneities notoriously difficult to detect by common techniques. Extending this work to the study of MOFs with different pore geometries (i.e., one-dimensional channel pores) may lead to a deeper understanding of the intimate relationship between pore geometry interconnectivity and Ps Bloch state characteristics.

This work was supported by the Swiss National Science Foundation (Grant No. PZ00P2_132059) and ETH Zurich (Grant No. ETH-47-12-1). B.B. is supported by the DOE Grants No. DE-FG02-07ER46352 and No. DE-AC02-05CH11231 for theory support at the Advanced Light Source, Berkeley, and the allocation of supercomputer time at NERSC. MOF synthesis was supported by the DOE (Grant No. DE-SC0004888). We are very grateful to A. Rubbia, K. Kirch, G. Dissertori, and the IPP at ETH Zurich for their essential support, to S. Eijt for very useful discussions, and to A. Gendotti and the IPP workshop for their help with the construction.

[1] M. Deutsch, *Phys. Rev.* **82**, 455 (1951).

[2] S. G. Karshenboim, *Phys. Rep.* **422**, 1 (2005).

[3] A. Badertscher, P. Crivelli, W. Fetscher, U. Gendotti, S. N. Gninenko, V. Postoev, A. Rubbia, V. Samoylenko, and D. Sillou, *Phys. Rev. D* **75**, 032004 (2007).

[4] A. P. Mills, *Phys. Rev. Lett.* **46**, 717 (1981).

[5] D. B. Cassidy and A. P. Mills, *Nature (London)* **449**, 195 (2007).

[6] B. Barbiellini and P. M. Platzman, *Phys. Status Solidi C* **6**, 2523 (2009).

- [7] D. W. Gidley, H. G. Peng, and R. S. Vallery, *Ann. Rev. Mater. Res.* **36**, 49 (2006).
- [8] W. Brandt, G. Coussot, and R. Paulin, *Phys. Rev. Lett.* **23**, 522 (1969).
- [9] A. Greenberger, A. P. Mills, A. Thompson, and S. Berko, *Phys. Lett. A* **32**, 72 (1970).
- [10] K. Inoue, N. Suzuki, I. V. Bondarev, and T. Hyodo, *Phys. Rev. B* **76**, 024304 (2007), and the references therein.
- [11] Y. Nagai, Y. Nagashima, and T. Hyodo, *Phys. Rev. B* **60**, 7677 (1999).
- [12] D. Dutta, J. I. Feldblyum, D. W. Gidley, J. Imirzian, M. Liu, A. J. Matzger, R. S. Vallery, and A. G. Wong-Foy, *Phys. Rev. Lett.* **110**, 197403 (2013).
- [13] C. Janiak and J. K. Vietha, *New J. Chem.* **34**, 2366 (2010).
- [14] O. K. Farha, I. Eryazici, N. C. Jeong, B. G. Hauser, C. E. Wilmer, A. A. Sarjeant, R. Q. Snurr, S. T. Nguyen, A. Ö. Yazaydin, and J. T. Hupp, *J. Am. Chem. Soc.* **134**, 15016 (2012).
- [15] T. A. Makal, J.-R. Li, W. Lu, and H.-C. Zhou, *Chem. Soc. Rev.* **41**, 7761 (2012).
- [16] M. Xue, Y. Liu, R. M. Schaffino, S. Xiang, X. Zhao, G. Zhu, S. Qiu, and B. Chen, *Inorg. Chem.* **48**, 4649 (2009).
- [17] H. Li, M. Eddaoudi, M. O’Keeffe, and O. M. Yaghi, *Nature (London)* **402**, 276 (1999).
- [18] M. Eddaoudi, J. Kim, N. Rosi, D. Vodak, J. Wachter, M. O’Keeffe, and O. M. Yaghi, *Science* **295**, 469 (2002).
- [19] J. L. C. Rowsell and O. M. Yaghi, *J. Am. Chem. Soc.* **128**, 1304 (2006).
- [20] N. Alberola, T. Anthonioz, A. Badertscher, C. Bas, A. S. Belov, P. Crivelli, S. N. Gninenko, N. A. Golubev, M. M. Kirsanov, A. Rubbia, and D. Sillou, *Nucl. Instrum. Methods Phys. Res., Sect. A* **560**, 224 (2006).
- [21] P. Crivelli, U. Gendotti, A. Rubbia, L. Liskay, P. Perez, and C. Corbel, *Phys. Rev. A* **81**, 052703 (2010).
- [22] See Supplemental Material at <http://link.aps.org/supplemental/10.1103/PhysRevB.89.241103> for PALS and TOF detector, simulation of the Ps emission and TOF distributions for all the studied MOFs.
- [23] A. P. Mills, Jr. and R. J. Wilson, *Phys. Rev. A* **26**, 490 (1982).
- [24] O. E. Mogensen, *J. Chem. Phys.* **60**, 998 (1974).
- [25] D. B. Cassidy, P. Crivelli, T. H. Hisakado, L. Liskay, V. E. Meline, P. Perez, H. W. K. Tom, and A. P. Mills, *Phys. Rev. A* **81**, 012715 (2010).
- [26] A. Antognini, P. Crivelli, T. Prokscha, K. S. Khaw, B. Barbiellini, L. Liskay, K. Kirch, K. Kwuida, E. Morenzoni, F. M. Piegsa, Z. Salman, and A. Suter, *Phys. Rev. Lett.* **108**, 143401 (2012).
- [27] L. Liskay, C. Corbel, L. Raboin, J.-P. Boilot, P. Perez, A. Brunet-Bruneau, P. Crivelli, U. Gendotti, A. Rubbia, T. Ohdaira, and R. Suzuki, *Appl. Phys. Lett.* **95**, 124103 (2009).
- [28] S. Agostinelli *et al.*, *Nucl. Instrum. Methods Phys. Res., Sect. A* **506**, 250 (2003).
- [29] D. B. Cassidy, T. H. Hisakado, V. E. Meline, H. W. K. Tom, and A. P. Mills, Jr., *Phys. Rev. A* **82**, 052511 (2010).
- [30] L. Di Noto, S. Mariazzi, M. Bettonte, G. Nebbia, and R. S. Brusa, *Eur. Phys. J. D* **66**, 118 (2012).
- [31] L. D. Landau and E. M. Lifshitz, *Quantum Mechanics* (Pergamon, New York, 1965), Vol. 3.
- [32] B. Barbiellini, S. B. Dugdale, and T. Jarlborg, *Comput. Mater. Sci.* **28**, 287 (2003).
- [33] The average size grain is $L_G = 300 \mu\text{m}$, therefore the smallest value for k is $2\pi/L_G$, which can safely be approximated to zero.
- [34] P. W. Anderson, *Phys. Rev.* **109**, 1492 (1958).
- [35] A. H. Baugher, W. J. Kossler, and K. G. Petzinger, *Macromolecules* **29**, 7280 (1996).
- [36] In our case, for the lowest band this is $BW \simeq 0.2 \text{ eV}$.
- [37] M. Grover and R. Silbey, *J. Phys. Chem.* **54**, 4843 (1971).
- [38] C. King, B. Barbiellini, D. Moser, and V. Renugopalakrishnan, *Phys. Rev. B* **85**, 125106 (2012).
- [39] I. V. Bondarev and T. Hyodo, *Phys. Rev. B* **57**, 11341 (1998).
- [40] T. Schaez, C. R. Monroe, and T. Esslinger, *New J. Phys.* **15**, 085009 (2013).
- [41] G. D. Scholes and C. Smyth, *J. Chem. Phys.* **140**, 110901 (2014).